Materials Advances

ROYAL SOCIETY OF CHEMISTRY

PAPER

View Article Online
View Journal | View Issue

Cite this: *Mater. Adv.*, 2023, 4, 1687

Luminescent protein–rare earth fluoride nanoflowers†

Wenyu Wei,[abc] Manman He,[a] Jianrui Ma,[a] Yirui Fan,[abc] Peng Liu*[bc] and Jianxi Xiao*[abc]

Received 1st January 2023,
Accepted 28th February 2023

DOI: 10.1039/d3ma00002h

rsc.li/materials-advances

Protein–inorganic hybrid nanomaterials are a new type of functional materials that combine the advantages of inorganic and organic polymers and nanomaterials. We herein report a simple one-pot method for synthesizing organic–inorganic hybrid nanoflowers under mild biomineralization conditions using proteins as an organic component and lanthanide fluorides as an inorganic component. The as-prepared protein–rare earth fluoride nanoflowers exhibit high performance in maintaining enzyme stability and catalytic activity due to their high surface area and graded nanostructures, and have finely tunable luminescence properties of lanthanide ions. Various proteins such as trypsin, BSA, collagen and FtsZ have all displayed excellent capability to produce $Na_5Yb_9F_{32}$ nanoflowers, demonstrating that protein-templated biomineralization provides a universal and robust strategy for the synthesis of protein–rare earth fluoride hybrid nanoflowers. The novel luminescent protein–rare earth fluoride nanoflowers may have promising applications in biosensing, biocatalysis and medical diagnostics and treatment.

Introduction

Nanomaterials with a higher surface area to volume ratio have been known to have superior advantages for improving the surface reaction efficiency compared to bulk materials. Nanoflowers as a newly developed class of nanoparticles with flower-like morphology have extraordinary features such as excellent catalytic ability, strong adsorption capacity, and efficient loading capability for multiple applications in catalysis, biosensors, and medicine, and have attracted the attention of scientists worldwide.[1–4] However, the synthesis of nanoflowers is an arduous task requiring harsh conditions in their making, including toxic organic reagents, high pressures, and high temperatures. Therefore, controlling the morphological characteristics of nanoflowers to tailor their structure is an intricate task, and applying these particles to the field of biochemistry is even more daunting.

Biomineralization is a remarkable strategy by which organisms phenomenally utilize the composition of organic and inorganic matrixes to produce functional materials with hierarchically ordered structures,[5–7] sparking inspiration for the design of novel materials. When using proteins as templates to synthesize $Cu_3(PO_4)_2{\cdot}3H_2O$ organic–inorganic hybrid nanoflowers, which possess a high surface-to-volume ratio, the immobilised proteases in the hybrid exhibit higher catalytic efficacy and better thermal stability compared to free proteases.[8] Recently, copper–protein,[9–12] calcium–protein,[13,14] manganese–protein hybrid nanoflowers,[15] copper–DNA hybrid nanoflowers,[16] and capsular hybrid nanoflowers[17,18] have been reported and have been shown to have many unexpected applications in catalysis,[19–21] biosensors,[22–25] and drug delivery.[26–29]

Rare earth nanoparticles (NPs) received intense interest due to their promising applications in biosensing,[30] photovoltaic devices,[31] near-infrared bioimaging[32] and photodynamic therapy.[33] In particular, rare earth fluoride NPs have attracted much attention, compared to their oxide counterparts. The fluoride host materials showed distinguished strengths such as low vibrational energies, low phonon energies and high chemical stability, endowing them as a research hotspot in the field of biomedicine. Rare earth fluoride nanomaterials have been used for various imaging studies by doping. For example, upconverting alkaline rare-earth fluorides doped with Yb^{3+} and Er^{3+} ions,[34] fluorescence-enhanced Yb^{3+}/Tm^{3+}-codoped fluoride[35] and Nd^{3+}/Yb^{3+}-codoped luminescent fluoride nanoparticles allowed high contrast time-gated *in vivo* NIR II window imaging.[36]

A variety of methods have been explored to create rare earth fluorides including chemical vapor deposition,[37] sol–gel processes,[38] microemulsion methods,[39] nonhydrolytic routes,[40]

[a] *State Key Laboratory of Applied Organic Chemistry, College of Chemistry and Chemical Engineering, Lanzhou University, Lanzhou 730000, P. R. China. E-mail: xiaojx@lzu.edu.cn*
[b] *Gansu Engineering Research Center of Medical Collagen, China. E-mail: pengliu@vacmic.com*
[c] *Joint Research Center of Collagen of Lanzhou University-China National Biotec Group, Lanzhou Biotechnology Development Co, China*

† Electronic supplementary information (ESI) available: Fig. S1–S3. See DOI: https://doi.org/10.1039/d3ma00002h

and hydrothermal processes,[41] while each approach suffered from its own drawbacks. For instance, the most used hydrothermal synthesis had low yield and required high-temperature conditions. The toxic organometallic precursors and organic solvents also raised serious concerns of potential environmental pollution. The development of innovative environmentally friendly methods for the synthesis of rare earth fluoride NPs with well-defined shapes and good dispersibility remains highly challenging, while the production of rare earth fluoride nanoflowers has not been reported yet.

Herein we have developed a novel protein-templated biomineralized strategy for the synthesis of monodisperse rare earth fluoride nanoflowers in an aqueous buffer at room temperature. This is a mild one-pot process for synthesizing organic–inorganic hybrid nanoflowers under biomineralization conditions. With this facile and safe synthesis method, it is possible to fabricate nanoflowers simply by adding proteins to rare earth fluoride solution and it does not require any toxic elements or extreme harsh conditions. The abundant presence of amide and carboxyl groups of proteins provides sites for the growth of rare earth fluoride crystals. The organic substance involved in the synthesis is subjected to less manipulation compared with other conventional methods to maintain the activity of the immobilized enzyme. Therefore, the immobilized proteases have been demonstrated to be far more stable and reusable than their free counterparts, and their catalytic activity became remarkably increased. The prepared protein–$Na_5Yb_9F_{32}$ nanoflowers display unique luminescence properties. The robust protein–rare earth fluoride nanoflowers may have promising applications in various fields such as biocatalysis, luminescent matrix materials, and medical diagnosis.

Experimental section

Materials

$YbN_3O_9{\cdot}5H_2O$, NaF, $Eu(NO_3)_3{\cdot}6H_2O$ and $Tb(NO_3)_3{\cdot}5H_2O$ were purchased from Aladdin. Trypsin was provided by Sangon Biotech. Bovine serum albumin (BSA) and Folin–Ciocalteu's phenol reagent were obtained from Solarbio. Casein was provided by Yuanye Bio-Technology. Urea, anhydrous sodium carbonate, and trichloroacetic acid (TCA) were obtained from Guangfu Fine Chemical. Collagen and FtsZ were expressed and purified according to the previously reported method.[42–44] All solvents were of reagent grade or HPLC grade.

Synthesis of protein–$Na_5Yb_9F_{32}$ hybrid nanoflowers

Trypsin–$Na_5Yb_9F_{32}$ hybrid nanoflowers were prepared from a mixture of 685 μL of trypsin solution (1.5 mg mL^{-1}) and 100 μL of $Yb(NO_3)_3$ solution (0.5 M). The reaction solution was stirred for 60 minutes to obtain a homogeneous mixture, and 300 μL of NaF solution (0.5 M) was then added and stirred for 10 minutes. The mixture was incubated for 12–36 hours at 25 °C. After centrifugation, the precipitates were washed three times using ethanol and air dried at room temperature. Other types of protein–$Na_5Yb_9F_{32}$ hybrid nanoflowers were obtained following similar protocols with different concentrations of proteins (6.0 mg mL^{-1} BSA; 6.0 mg mL^{-1} collagen; and 1.5 mg mL^{-1} Ftsz).

Characterization of trypsin–$Na_5Yb_9F_{32}$ hybrid nanoflowers

The X-ray diffraction (XRD) images of the synthesised hybrid nanomaterials were obtained using a Rigaku D/ma-2500 diffractometer with Cu Kα radiation (40 kV, 200 mA) at a scanning rate of 0.02° s^{-1} in the 2θ range from 10° to 90°. X-ray photoelectron spectroscopy (XPS) patterns were recorded using a Kaltos Axis UltraDLD X-ray photoelectron spectroscope (Kratos Analytical, Manchester, UK) with a monochrome X-ray source using Alkα (1486.6 eV) radiation. The binding energies were measured and corrected by referencing the C 1s line at 284.5 eV. Fourier-transform infrared (FT-IR) spectra were measured using a Nicolet NEXUS 670 infrared spectrometer. Thermogravimetric analysis (TGA) was carried out on a TGA/NETZSCH STA449F3 instrument under a nitrogen atmosphere with a heating rate of 10 °C min^{-1} from 25 °C to 800 °C. Scanning Electron Microscopy (SEM) experiments were performed on a Hitachi S-4800 field emission scanning electron microscope (Hitachi Limited, Japan). TEM (transmission electron microscopy), HRTEM (high-resolution transmission electron microscopy), SAED (selected area electron diffraction), and electron diffraction (EDX) were performed at 200 kV using a JEM-2100 transmission electron microscope (JEOL, Japan). The specific surface area and pore size of the nanoflowers were analysed by the Brunauer–Emmett–Teller (BET) and Barrett–Joyner–Halenda (BJH) methods using a physisorption analyzer (Micromeritics ASAP2020 porosimeter, USA).

Photoluminescence spectroscopy

Using a Xe lamp as the excitation source, photoluminescence emission spectra were acquired on a FLS920 fluorescence spectrophotometer (Edinburgh Instruments, England). The emission spectra were recorded for the protein–$Na_5Yb_9F_{32}$:Tb^{3+} (or Eu^{3+}) aggregates at λ_{ex} = 369 nm and λ_{ex} = 394 nm, respectively.

The enzymatic activity of trypsin–$Na_5Yb_9F_{32}$ hybrid nanoflowers and free trypsin

The Folin assay was used to determine the enzymatic activity of trypsin–$Na_5Yb_9F_{32}$ hybrid nanoflowers. Casein was used as a substrate. Casein solution (10 g L^{-1}) was prepared in PBS buffer (50 mM, pH 7.4). Trypsin–$Na_5Yb_9F_{32}$ (10 mg) was added to casein (1 mL, 10 g L^{-1}) and incubated at 30 °C for 30 minutes. The supernatant was collected after centrifugation for 5 minutes (9000 rpm). 2 mL of TCA solution (0.4 M) was added to the supernatant for 5 minutes. After centrifugation, the supernatant was harvested. 5 mL of Na_2CO_3 solution (0.4 M) and 1 mL of Ciocalteu's phenol reagent were mixed with 1 mL of the supernatant. To complete the color development reaction, the mixture solution was incubated at 40 °C for 20 minutes. The absorbance at 763 nm was monitored to evaluate the casein hydrolysis performance. The activity of free trypsin was assessed by the same procedure using the corresponding amount of trypsin in the hybrid nanoflowers.

The enzymatic profiles of trypsin–$Na_5Yb_9F_{32}$ and free trypsin under denatured conditions were investigated in the presence of different amounts of urea or ACN. In order to investigate the thermal stability of trypsin–$Na_5Yb_9F_{32}$ and free trypsin, their enzymatic activities were simultaneously monitored at 55 °C at different time intervals for 10 h using the Folin assay. Meanwhile, the enzymatic activities of trypsin–$Na_5Yb_9F_{32}$ and free trypsin were measured at various temperatures (40–55 °C). The relative activities of trypsin–$Na_5Yb_9F_{32}$ and free trypsin at different temperatures were normalised to the value at 40 °C.

The reusability of trypsin–$Na_5Yb_9F_{32}$ hybrid nanoflowers

The reusability of trypsin–$Na_5Yb_9F_{32}$ was investigated by recombinant collagen (V-CL) digestion assay as previously described.[45] Briefly, recombinant collagen V-CL (5 mg mL^{-1}, 50 mM glycine buffer, pH 8.6) was incubated with 2 mg of trypsin–$Na_5Yb_9F_{32}$ at 25 °C for ~12 hours. The supernatant was obtained by centrifugation and stored at −20 °C. The precipitates were washed three times with a glycine buffer and then reused for another cycle. The VCL cleavage experiments were carried out eight times following the same procedure. All the collected supernatants were used for SDS-PAGE analysis.

Results and discussion

Synthesis and characterization of trypsin–$Na_5Yb_9F_{32}$ hybrid nanoflowers

Trypsin–$Na_5Yb_9F_{32}$ hybrid nanomaterials were produced by incubating a mixture of trypsin (0.95 mg mL^{-1}), $Yb(NO_3)_3$ (46 mM) and NaF (138 mM) at 25 °C for 12 hours. The crystallinity of the nanomaterials was characterised by the XRD (X-ray diffraction) technique, and their diffraction profiles were consistent with $Na_5Yb_9F_{32}$ (JCPDS No. 27-1426) (Fig. 1a). The elemental composition of the nanomaterials was determined by XPS (X-ray photoelectron spectroscopy), and it indicated the presence of C, N, O, Na, Yb and F elements, which corresponded to proteins and $Na_5Yb_9F_{32}$, respectively (Fig. 1b). These results demonstrated that trypsin provides a good bio template to create pure $Na_5Yb_9F_{32}$ rare earth fluoride crystals under mild incubation conditions.

The FT-IR spectra of hybrid nanomaterials displayed a strong IR band at 1384 cm^{-1}, which corresponded to the characteristic absorption of the Yb–F bond of $Na_5Yb_9F_{32}$ (Fig. 1c). The observed vibration peaks at 2964 cm^{-1} and 1537 cm^{-1} were ascribed to the C–H and N–H bonds, respectively, suggesting the presence of trypsin within the synthesised $Na_5Yb_9F_{32}$ crystal (Fig. 1c). The content of trypsin in the hybrid nanomaterials was further estimated by thermogravimetric analysis (TGA) (Fig. 1d). The TGA curve showed three stages of weight loss: loss of water below 200 °C, thermal decomposition of protein between 200 and 650 °C, and decomposition of $Na_5Yb_9F_{32}$ above 650 °C. It indicated that approximately 2.09% of trypsin was encapsulated in the hybrid nanomaterials (Fig. 1d). All these results indicated that the mild incubation of the mixture of trypsin, $Yb(NO_3)_3$ and NaF led to the production of hybrid trypsin–$Na_5Yb_9F_{32}$ nanomaterials using trypsin as the bio template.

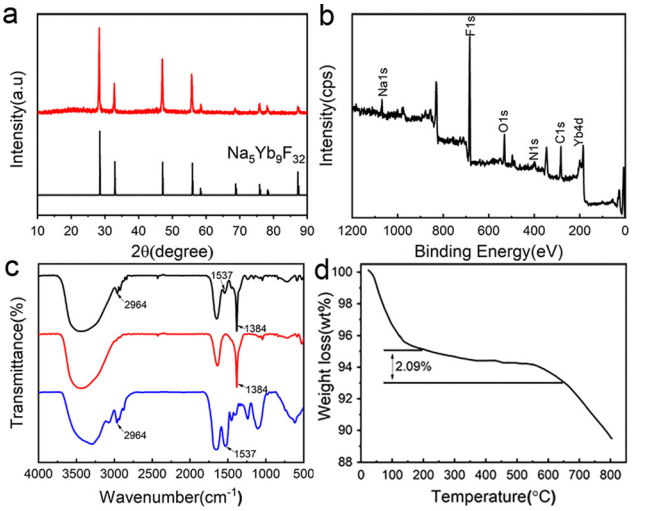

Fig. 1 XRD (a), XPS (b), FT-IR (c), and TGA (d) characterization of the prepared trypsin–$Na_5Yb_9F_{32}$ hybrid nanomaterials. The XRD pattern of the standard $Na_5Yb_9F_{32}$ crystal (black) is shown below the plot of the hybrid nanomaterials (red) (a). FT-IR spectra of trypsin–$Na_5Yb_9F_{32}$ hybrid nanomaterial (black), $Na_5Yb_9F_{32}$ (red), and trypsin (blue) (c).

Field emission scanning electron microscopy (FESEM) and transmission electron microscopy (TEM) techniques were performed to determine the morphology and detailed structure of the hybrid trypsin–$Na_5Yb_9F_{32}$ nanomaterials. SEM images showed that the nanomaterials exhibited a carnation-like nanoflower structure with a diameter of approximately 3 μm (Fig. 2a). The magnified SEM image of the hybrid nanoflowers indicated that they have a layered structure with a high surface area to volume ratio, which was assembled by individual nanoparticle units (Fig. 2b). The TEM image further showed that the $Na_5Yb_9F_{32}$ crystals were assembled *via* an oriented attachment of primary nanoparticles (Fig. 2c). The HRTEM image showed the characteristic (111) lattice spacing (0.31 nm) of the rare earth fluoride $Na_5Yb_9F_{32}$ crystals (Fig. 2d). The pattern of selected-area electron diffraction (SAED) indicated that the assembly of primary $Na_5Yb_9F_{32}$ nanoparticles was quite oriented (Fig. 2d).

The presence of C, N, Na, Yb and F was evident in the energy dispersive X-ray (EDX) analysis of hybrid nanomaterials (Fig. 2e). The high angle annular dark field scanning TEM (HAADF-STEM) image indicated that the primary $Na_5Yb_9F_{32}$ nanoparticles gradually aggregated to form hierarchical flower-like mesocrystals (Fig. 2f). The corresponding element mapping results of energy dispersive X-ray spectroscopy (EDS) further showed that the C, Na, F and Yb elements were evenly distributed on the hybrid nanoflowers (Fig. 2g). In addition, the Brunauer–Emmett–Teller (BET) surface area and average pore size of the $Na_5Yb_9F_{32}$ mesocrystals were calculated using the Barrett–Joyner–Halenda (BJH) model to be 86.8 m^2 g^{-1} and 231.0 Å, respectively (Fig. S1, ESI†). It is demonstrated that the $Na_5Yb_9F_{32}$ mesocrystals displayed a porous structure with a high surface-to-volume ratio. All the results indicated that the

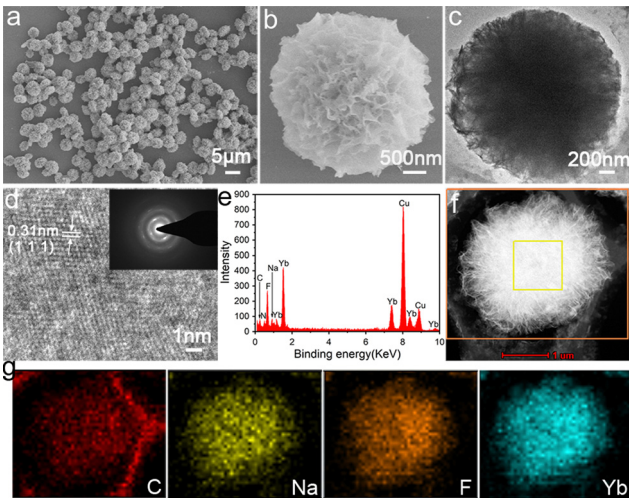

Fig. 2 Electron microscopy characterization of the morphology of trypsin–$Na_5Yb_9F_{32}$ hybrid nanomaterials. FESEM images of trypsin–$Na_5Yb_9F_{32}$ nanoflowers prepared by the incubation of the mixture of trypsin (0.95 mg mL^{-1}), $Yb(NO_3)_3$ (46 mM) and NaF (138 mM) at 25 °C for 48 h (a and b). TEM image (c), HRTEM image, SAED pattern (inset) (d), EDX spectrum (e), and HAADF-STEM image (f) of the trypsin–$Na_5Yb_9F_{32}$ nanoflowers. (g) EDS mapping images of C, Na, F, and Yb for the square region of the $Na_5Yb_9F_{32}$ particles in (f).

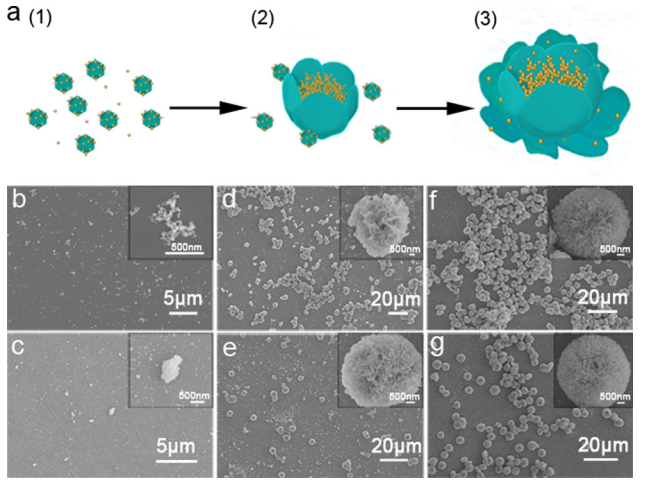

Fig. 3 (a) Schematic representation of the formation mechanism of trypsin–$Na_5Yb_9F_{32}$ hybrid nanoflowers. FESEM images of trypsin–$Na_5Yb_9F_{32}$ hybrid nanomaterials prepared at different incubation times: 5 min (b), 30 min (c), 3 h (d), 5 h (e), 12 h (f) and 36 h (g).

trypsin-templated biomineralization process resulted in $Na_5Yb_9F_{32}$ mesocrystals with elegant flower-like morphology.

Time-dependent evolution of trypsin–$Na_5Yb_9F_{32}$ hybrid nanoflowers

The time-dependent evolution of trypsin–$Na_5Yb_9F_{32}$ hybrid nanoflowers was monitored by SEM and XRD to investigate the underlying mechanism of biomineralization of $Na_5Yb_9F_{32}$ crystals using trypsin as the template (Fig. 3 and Fig. S2, ESI†). A mixture of trypsin (0.95 mg mL^{-1}), $Yb(NO_3)_3$ (46 mM) and NaF (138 mM) was incubated at 25 °C. SEM images as a function of time suggested the following formation mechanism of trypsin–$Na_5Yb_9F_{32}$ hybrid nanoflowers (Fig. 3a). At the early growth step, Yb(III) ions formed a complex with trypsin probably through the interaction of charged amino acids, leading to the production of primary crystals (Fig. 3b and c). At the secondary growth step, the primary $Na_5Yb_9F_{32}$ crystals self-assembled to form nanoflowers with small petals, while trypsin probably covered the surface and stabilized the primary crystals (Fig. 3d and e). At the final anisotropic growth step, the nanoparticles continued the oriented-assembly to build hierarchical flower-like mesocrystals with branched petals (Fig. 3f and g). In this time-dependent biomineralization process for the production of hybrid nanoflowers, trypsin played a key role by guiding the nucleation of $Na_5Yb_9F_{32}$ to form a well-ordered scaffold and gluing the petals together (Fig. 3a). Meanwhile, the nanomaterials obtained at different times of incubation (5 min, 30 min, 3 h, 5 h, 12 h and 36 h) showed the same XRD pattern assigned to pure $Na_5Yb_9F_{32}$ crystals (JCPDS No. 27-1426) (Fig. S2, ESI†). This indicated that the mixture formed primary $Na_5Yb_9F_{32}$ crystals at the initial stage and kept the same crystal phase during the growth of trypsin–$Na_5Yb_9F_{32}$ hybrid nanoflowers.

In order to examine the critical role of trypsin in the generation of hybrid nanoflowers, the morphologies of trypsin–$Na_5Yb_9F_{32}$ hybrid nanomaterials were measured after treatments with calcination and glutaraldehyde/EDTA (Fig. S3, ESI†). Calcination of the as-prepared hybrid nanomaterials at 350 °C for 6 h resulted in the disruption of flower-like structures, suggesting that trypsin was a key factor to hold the hierarchical structure (Fig. S3a, ESI†). When the hybrid nanomaterials were first cross-linked by glutaraldehyde and then treated with ethylenediaminetetraacetic acid (EDTA) to remove the Yb^{3+} ions, the exquisite nanoflower morphology was also destroyed, suggesting that the Yb^{3+} ions were also critical in the formation of nanoflowers (Fig. S3b, ESI†). These results demonstrated that both trypsin and Yb^{3+} ions were evenly distributed in the hybrid nanomaterials, and they collectively regulated the morphology of hybrid nanoflowers.

Universality of protein–$Na_5Yb_9F_{32}$ nanoflowers

In order to evaluate the general applicability of the production of $Na_5Yb_9F_{32}$ crystals using proteins as the template, different types of proteins were used for the biomineralization process and the morphology of the as-prepared hybrid nanomaterials was characterised by SEM (Fig. 4). In the absence of proteins, the synthesised nanomaterials formed small nanospheres with a diameter of approximately 350 nm (Fig. 4a). Collagen and FtsZ were prepared by recombinant methods as previously described.[42–44] When BSA, collagen or FtsZ was added, the generated nanomaterials displayed well-ordered flower-like nanostructures. In summary, different types of proteins could be used as bio templates to create hybrid protein–$Na_5Yb_9F_{32}$ hybrid nanoflowers.

Enzymatic activity of trypsin–$Na_5Yb_9F_{32}$ hybrid nanoflowers

The enzymatic activity of trypsin–$Na_5Yb_9F_{32}$ hybrid nanoflowers and free trypsin was evaluated using the Folin assay. Urea and

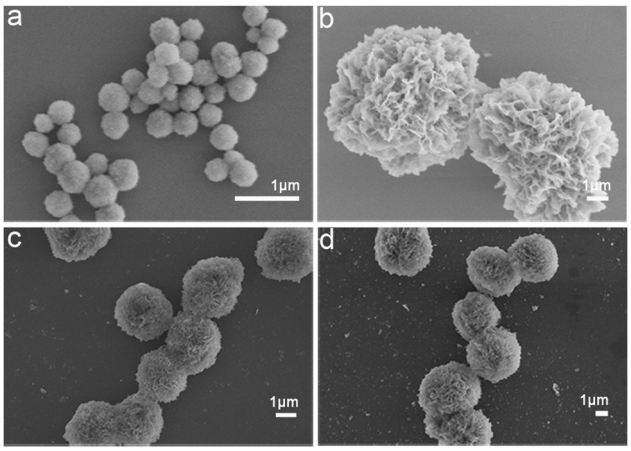

Fig. 4 FESEM images of protein–$Na_5Yb_9F_{32}$ hybrid nanomaterials prepared by using different types of proteins as the biotemplates: (a) no protein; (b) BSA; (c) collagen; and (d) FtsZ.

ACN are widely used to denature native proteins in proteomics experiments. Therefore, different concentrations of urea and ACN were added to the casein solution to investigate the performance of trypsin–$Na_5Yb_9F_{32}$ and free trypsin under denaturing conditions (Fig. 5a and b). When compared to free trypsin, trypsin–$Na_5Yb_9F_{32}$ nanomaterials displayed higher relative activity in the presence of a large amount of urea or ACN (Fig. 5a and b). This indicated that trypsin–$Na_5Yb_9F_{32}$ had high tolerance to denaturing conditions.

The enzymatic activity of trypsin–$Na_5Yb_9F_{32}$ nanoflowers and free trypsin was measured at various temperatures to evaluate their thermal stability. The activities of trypsin–$Na_5Yb_9F_{32}$ and free trypsin at different temperatures were normalised to that at 40 °C as relative activity for comparison. When the temperature was higher than 40 °C, the synthesised trypsin–$Na_5Yb_9F_{32}$ nanoflowers possessed a much higher relative activity than free trypsin, indicating high tolerance of trypsin–$Na_5Yb_9F_{32}$ towards inactivation due to high temperature (Fig. 5c).

The enzymatic activity of trypsin–$Na_5Yb_9F_{32}$ nanoflowers and free trypsin was also real-time monitored at 55 °C (Fig. 5d). The activity of free trypsin was significantly reduced after 3 h of incubation, while the trypsin–$Na_5Yb_9F_{32}$ nanoflowers always maintained much higher enzymatic activity during the whole time of incubation, indicating high heat resistance of trypsin–$Na_5Yb_9F_{32}$ (Fig. 5d). These results indicated that the trypsin–$Na_5Yb_9F_{32}$ nanoflowers possessed good stability against thermal and chemical denaturation. It may be due to the increased stability of immobilised enzymes on the metal surface and enhanced mass transfer due to the high surface areas of nanoflowers.

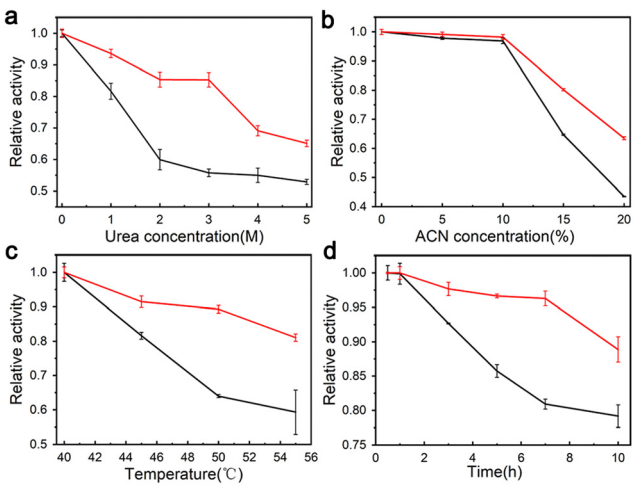

Fig. 5 Enzymatic activity of trypsin–$Na_5Yb_9F_{32}$ hybrid nanoflowers (red) and free trypsin (black) under different conditions. Enzymatic activity was measured under denaturing conditions by adding various concentrations of urea (a) and acetonitrile (ACN) (b). Enzymatic activity was determined at different incubation temperatures (c) and different incubation times at 55 °C (d).

Reusability of trypsin–$Na_5Yb_9F_{32}$ hybrid nanoflowers

The reusability of trypsin–$Na_5Yb_9F_{32}$ hybrid nanoflowers was investigated using recombinant collagen V-CL, a good model system for visualizing the enzymatic cleavage activity of trypsin. The V-domain is easily digested by trypsin when it is below the melting temperature of V-CL (37 °C), whereas the CL domain is resistant to trypsin cleavage. Therefore, the digested product of V-CL showed a single band of CL in SDS-PAGE, making it a convenient method for detecting the activity and reusability of trypsin–$Na_5Yb_9F_{32}$. SDS-PAGE experiments showed that the V-CL protein from the control sample migrated to a single band around 45 kDa, whereas the addition of trypsin–$Na_5Yb_9F_{32}$ caused the digested product of CL to migrate as another single band, demonstrating that V-CL was completely digested by trypsin-$Na_5Yb_9F_{32}$ (Fig. 6). After repeated use of 8 cycles, the trypsin–$Na_5Yb_9F_{32}$ hybrid nanoflowers maintained similarly high activity to completely cleave V-CL (Fig. 6). In conclusion, trypsin–$Na_5Yb_9F_{32}$ hybrid nanoflowers had excellent reusability, which was one of the most favoured properties of immobilised enzymes.

Photoluminescence of trypsin–$Na_5Yb_9F_{32}$ hybrid nanoflowers

Lanthanide ion-doped luminescent materials have been widely used in bioimaging and optoelectronics because of their low toxicity, large Stokes shift, and strong resistance to photodegradation. The photoluminescence properties of trypsin–$Na_5Yb_9F_{32}$ hybrid nanoflowers doped with Tb^{3+} and Eu^{3+} were characterised using a solid state fluorescence spectrometer

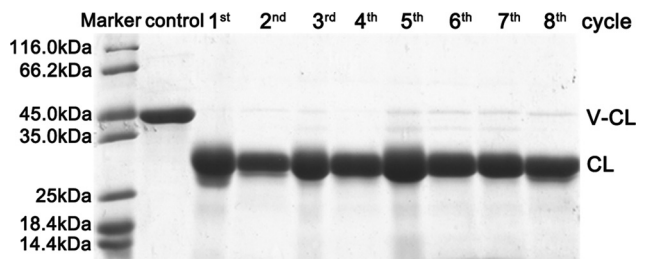

Fig. 6 SDS-PAGE analysis of the repeated use of trypsin–$Na_5Yb_9F_{32}$ hybrid nanoflowers towards the cleavage of recombinant collagen (V-CL).

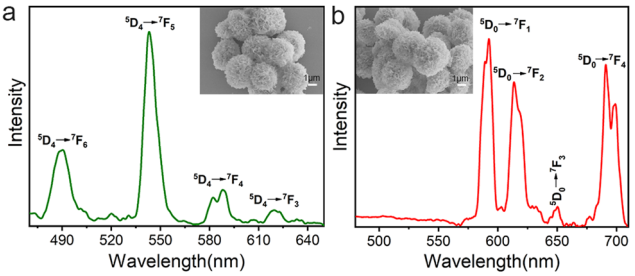

Fig. 7 Emission spectra of luminescent materials of trypsin–$Na_5Yb_9F_{32}$ doped with specified lanthanide ions: (a) Tb^{3+} and (b) Eu^{3+}. The emission spectra were recorded at λ_{ex} = 369 nm and λ_{ex} = 394 nm for Tb^{3+} and Eu^{3+}, respectively. SEM images of the doped hybrid nanomaterials are shown in the insets.

(Fig. 7). A mixture of trypsin (0.95 mg mL^{-1}), $Yb(NO_3)_3$ (46 mM), NaF (138 mM) and $Tb(NO_3)_3$ (or $Eu(NO_3)_3$, 5 mM) was incubated at 25 °C for 12 hours to obtain trypsin–$Na_5Yb_9F_{32}$:Tb^{3+} and trypsin–$Na_5Yb_9F_{32}$:Eu^{3+} nanoflowers, respectively. The SEM images of the doped nanopowders indicated that the addition of Eu or Tb does not affect the final morphology and the doped samples have the same flower-like morphology as undoped trypsin–$Na_5Yb_9F_{32}$. The emission spectrum of the as-prepared Tb-doped trypsin–$Na_5Yb_9F_{32}$ nanoflowers at an excitation wavelength of 369 nm showed a strong green emission at ~543 nm along with other weak emission lines which can be attributed to intra-configurational f–f transitions of Tb^{3+} ions. The observed emission lines at 490, 543, 588 and 620 nm were ascribed to the intra-$^4f_8$ transitions from the $^5D_4$ energy level to $^7F_6$, $^7F_5$, $^7F_4$ and $^7F_3$ energy levels, respectively.[46] Similarly, Fig. 7b shows the room-temperature photoluminescence emission spectrum of Eu-doped trypsin–$Na_5Yb_9F_{32}$ nanoflowers under 369 nm laser excitation. It displayed multiple emission peaks at 593, 614, 650 and 691 nm ascribed to the intra-$^4f_6$ transitions from the lowest excited $^5D_0$ level to the $^7F_1$, $^7F_2$, $^7F_3$ and $^7F_4$ levels, respectively.[47–50] These results showed that the protein–inorganic $Na_5Yb_9F_{32}$ nanomaterials displayed good photoluminescence features and their colours could be easily adjusted by using different kinds of lanthanide ions.

Conclusions

Nanoflowers are a novel type of nanoparticles with superior features such as high surface area and strong adsorption capacity and have attracted increasing attention in the fields of catalysis, biosensors, and medicine. Rare earth fluoride nanoparticles display fabulous advantages such as low phonon energies and high chemical stability and have been extensively used in biosensing and photovoltaic devices. However, the fabrication of rare earth fluoride nanoparticles with flower-like morphology remains an unmet demand.

We have for the first time developed well-ordered protein–rare earth fluoride nanoflowers using trypsin as the unique template for biomineralization. The XRD and XPS graphs indicated that pure $Na_5Yb_9F_{32}$ rare earth fluoride crystals were achieved *via* this trypsin-templated biomineralization process, while the SEM and TEM images demonstrated that the as-prepared $Na_5Yb_9F_{32}$ mesocrystals possess exquisite flower-like architecture. The FT-IR and TGA characterization confirmed the encapsulation of trypsin in the $Na_5Yb_9F_{32}$ mesocrystals. The time-dependent evolution of trypsin–$Na_5Yb_9F_{32}$ hybrid nanoflowers suggested that trypsin played a vital role by guiding the nucleation of $Na_5Yb_9F_{32}$ to form a well-ordered scaffold and cohering the petals together.

Enzymatic studies indicated that in contrast to free trypsin, the trypsin–$Na_5Yb_9F_{32}$ nanoflowers display excellent stability against thermal and chemical denaturation. Notably, the immobilized trypsin has superior re-usability. Furthermore, the trypsin–$Na_5Yb_9F_{32}$ nanomaterials display excellent photoluminescence features and their colours could be easily tuned by using different kinds of lanthanide ions. The one-pot environmentally amiable biomineralization approach leads to the production of multifunctional trypsin–$Na_5Yb_9F_{32}$ hybrid nanoflowers combining the attractive optical and catalytic features of rare earth fluorides and trypsin, respectively.

Different proteins such as BSA, collagen and FtsZ have all shown remarkable capability to create flower-like nanoparticles, suggesting that protein-templated biomineralization provides a universal and robust approach for the synthesis of protein–rare earth fluoride hybrid nanoflowers. The novel luminescent protein–rare earth fluoride nanoflowers may have great potential in biosensors, industrial biocatalysis and medical diagnostic technologies.

Conflicts of interest

The authors declare no competing conflicts of interest.

Acknowledgements

This work was supported by grants from the National Natural Science Foundation of China (grant no. 22074057 and 21775059) and the Natural Science Foundation of Gansu Province (grant no. 20YF3FA025 and 18YF1NA004).

References

1 J. Zeng and Y. Xia, *Nat. Nanotechnol.*, 2012, **7**, 415–416.
2 J. L. Wang, X. Q. You, C. Xiao, X. P. Zhang, S. H. Cai, W. L. Jiang, S. S. Guo, S. H. Cao and Z. Chen, *Appl. Catal., B*, 2019, **259**, 118060.
3 C. C. Zhai, L. Y. Miao, Y. B. Zhang, L. Q. Zhang, H. Li and S. X. Zhang, *Chem. Eng. J.*, 2022, **431**, 134107.
4 T. Yin, Y. J. Li, K. X. Bian, R. Y. Zhu, Z. W. Liu, K. Niu, H. Liu, Z. R. Gao and D. W. Gao, *Mater. Sci. Eng., C*, 2018, **93**, 716–723.
5 L. C. Palmer, C. J. Newcomb, S. R. Kaltz, E. D. Spoerke and S. I. Stupp, *Chem. Rev.*, 2008, **108**, 4754–4783.
6 P. Fratzl, O. Kolednik, F. D. Fischer and M. N. Dean, *Chem. Soc. Rev.*, 2016, **45**, 252–267.
7 L. B. Gower, *Chem. Rev.*, 2008, **108**, 4551–4627.

8 J. Ge, J. D. Lei and R. N. Zare, *Nat. Nanotechnol.*, 2012, **7**, 428–432.
9 L. Zhu, L. Gong, Y. F. Zhang, R. Wang, J. Ge, Z. Liu and R. N. Zare, *Chem. – Asian J.*, 2013, **8**, 2358–2360.
10 J. Y. Sun, J. C. Ge, W. M. Liu, M. H. Lan, H. Y. Zhang, P. F. Wang, Y. M. Wang and Z. W. Niu, *Nanoscale*, 2014, **6**, 255–262.
11 Z. Lin, Y. Xiao, L. Wang, Y. Q. Yin, J. N. Zheng, H. H. Yang and G. N. Chen, *RSC Adv.*, 2014, **4**, 13888–13891.
12 Z. Lin, Y. Xiao, Y. Q. Yin, W. L. Hu, W. Liu and H. H. Yang, *ACS Appl. Mater. Interfaces*, 2014, **6**, 10775–10782.
13 L. B. Wang, Y. C. Wang, R. He, A. Zhuang, X. P. Wang, J. Zeng and J. G. Hou, *J. Am. Chem. Soc.*, 2013, **135**, 1272–1275.
14 X. L. Wang, J. F. Shi, Z. Li, S. H. Zhang, H. Wu, Z. Y. Jiang, C. Yang and C. Y. Tian, *ACS Appl. Mater. Interfaces*, 2014, **6**, 14522–14532.
15 Z. H. Zhang, Y. C. Zhang, R. R. Song, M. H. Wang, F. F. Yan, L. H. He, X. Z. Feng, S. M. Fang, J. H. Zhao and H. Z. Zhang, *Sens. Actuators, B*, 2015, **211**, 310–317.
16 R. Hu, X. B. Zhang, Z. L. Zhao, G. Z. Zhu, T. Chen, T. Fu and W. H. Tan, *Angew. Chem., Int. Ed.*, 2014, **53**, 5821–5826.
17 J. F. Shi, S. H. Zhang, X. L. Wang, C. Yang and Z. Y. Jiang, *J. Mater. Chem. B*, 2014, **2**, 4289–4296.
18 K. Li, J. H. Wang, Y. J. He, M. A. Abdulrazaq and Y. J. Yan, *J. Biotechnol.*, 2018, **281**, 87–98.
19 G. K. Kouassi, J. Irudayaraj and G. McCarty, *J. Nanobiotechnol.*, 2005, **3**, 1.
20 R. S. Prakasham, G. S. Devi, C. S. Rao, V. S. S. Sivakumar, T. Sathish and P. N. Sarma, *Appl. Biochem. Biotechnol.*, 2010, **160**, 1888–1895.
21 S. A. Ansari and Q. Husain, *Biotechnol. Adv.*, 2012, **30**, 512–523.
22 J. Njagi and S. Andreescu, *Biosens. Bioelectron.*, 2007, **23**, 168–175.
23 J. H. Lin, W. Qu and S. S. Zhang, *Anal. Biochem.*, 2007, **360**, 288–293.
24 Y. W. Zhang, Y. Zhang, H. Wang, B. Yan, G. L. Shen and R. Q. Yu, *J. Electroanal. Chem.*, 2009, **627**, 9–14.
25 P. Takhistov, *Biosens. Bioelectron.*, 2004, **19**, 1445–1456.
26 R. X. Wang, Z. G. Tian and L. Y. Chen, *Int. J. Pharm.*, 2011, **406**, 153–162.
27 P. S. Kumar, S. Ramakrishna, T. R. Saini and P. V. Diwan, *Pharmazie*, 2006, **61**, 613–617.
28 P. Wanakule, G. W. Liu, A. T. Fleury and K. Roy, *J. Controlled Release*, 2012, **162**, 429–437.
29 J. K. Kim, J. Anderson, H. W. Jun, M. A. Repka and S. Jo, *Mol. Pharmaceutics*, 2009, **6**, 978–985.
30 K. J. McHugh, L. H. Jing, S. Y. Severt, M. Cruz, M. Sarmadi, H. S. N. Jayawardena, C. F. Perkinson, F. Larusson, S. Rose, S. Tomasic, T. Graf, S. Y. Tzeng, J. L. Sugarman, D. Vlasic, M. Peters, N. Peterson, L. Wood, W. Tang, J. Yeom, J. Collins, P. A. Welkhoff, A. Karchin, M. Tse, M. Y. Gao, M. G. Bawendi, R. Langer and A. Jaklenec, *Sci. Transl. Med.*, 2019, **11**, eaay7162.
31 W. G. J. H. M. van Sark, J. de Wild, J. K. Rath, A. Meijerink and R. E. I. Schropp, *Nanoscale Res. Lett.*, 2013, **8**, 81.
32 Y. T. Zhong, Z. R. Ma, F. F. Wang, X. Wang, Y. J. Yang, Y. L. Liu, X. Zhao, J. C. Li, H. T. Du, M. X. Zhang, Q. H. Cui, S. J. Zhu, Q. C. Sun, H. Wan, Y. Tian, Q. Liu, W. Z. Wang, K. C. Garcia and H. J. Dai, *Nat. Biotechnol.*, 2019, **37**, 1322.
33 D. D. Zhang, L. W. Wen, R. Huang, H. H. Wang, X. L. Hu and D. Xing, *Biomaterials*, 2018, **153**, 14–26.
34 T. Grzyb and D. Przybylska, *Inorg. Chem.*, 2018, **57**, 6410–6420.
35 H. L. Qiu, C. H. Yang, W. Shao, J. Damasco, X. L. Wang, H. Agren, P. N. Prasad and G. Y. Chen, *Nanomaterials*, 2014, **4**, 55–68.
36 M. L. Tan, B. del Rosal, Y. Q. Zhang, E. M. Rodriguez, J. Hu, Z. G. Zhou, R. W. Fan, D. H. Ortgies, N. Fernandez, I. Chaves-Coira, A. Nunez, D. Jaque and G. Y. Chen, *Nanoscale*, 2018, **10**, 17771–17780.
37 Q. G. Meng, R. J. Witte, P. S. May and M. T. Berry, *Chem. Mater.*, 2009, **21**, 5801–5808.
38 V. Sudarsan, S. Sivakumar, F. C. J. M. van Veggel and M. Raudsepp, *Chem. Mater.*, 2005, **17**, 4736–4742.
39 T. Aubert, F. Grasset, S. Mornet, E. Duguet, O. Cador, S. Cordier, Y. Molard, V. Demange, M. Mortier and H. Haneda, *J. Colloid Interface Sci.*, 2010, **341**, 201–208.
40 P. H. Mutin and A. Vioux, *Chem. Mater.*, 2009, **21**, 582–596.
41 X. Wang, J. Zhuang, Q. Peng and Y. D. Li, *Inorg. Chem.*, 2006, **45**, 6661–6665.
42 A. Yoshizumi, Z. Yu, T. Silva, G. Thiagarajan, J. A. Ramshaw, M. Inouye and B. Brodsky, *Protein Sci.*, 2009, **18**, 1241–1251.
43 J. C. Munyemana, H. He, S. Ding, J. Yin, P. Xi and J. Xiao, *RSC Adv.*, 2018, **8**, 2708–2713.
44 F. Yang, S. Zhang, S. Ding, Y. Hou, L. Yu, X. Chen and J. Xiao, *Int. J. Biol. Macromol.*, 2016, **91**, 294–298.
45 X. Sun, X. Cai, R. Q. Wang and J. Xiao, *Anal. Biochem.*, 2015, **477**, 21–27.
46 H. Lai, A. Bao, Y. Yang, Y. Tao, H. Yang, Y. Zhang and L. Han, *J. Phys. Chem. C*, 2008, **112**, 282–286.
47 S. Rodriguez-Liviano, F. J. Aparicio, T. C. Rojas, A. B. Hungría, L. E. Chinchilla and M. Ocaña, *Cryst. Growth Des.*, 2012, **12**, 635–645.
48 H. Guo, F. Li, J. Li and H. Zhang, *J. Am. Ceram. Soc.*, 2011, **94**, 1651–1653.
49 X. Yang, X. Dong, J. Wang and G. Liu, *Mater. Lett.*, 2009, **63**, 629–631.
50 S. Majeed, M. Bashir and S. Shivashankar, *J. Nanopart. Res.*, 2015, **17**, 1–15.